

Assignment of pre-edge features in the Ru K-edge X-ray absorption spectra of organometallic ruthenium complexes

Kendra Getty, Mario Ulises Delgado-Jaime, Pierre Kennepohl *

Department of Chemistry, The University of British Columbia, Vancouver BC, Canada V6T 1Z1

Received 29 June 2007; accepted 31 July 2007

Available online 7 August 2007

In recognition of the scientific leadership and mentorship of Professor Edward I. Solomon on the occasion of his 60th birthday.

Abstract

The nature of the lowest energy bound-state transition in the Ru K-edge X-ray absorption spectra for a series of Grubbs-type ruthenium complexes was investigated. The pre-edge feature was unambiguously assigned as resulting from formally electric dipole forbidden Ru 4d \leftarrow 1s transitions. The intensities of these transitions are extremely sensitive to the ligand environment and the symmetry of the metal centre. In centrosymmetric complexes the pre-edge is very weak since it is limited by the weak electric quadrupole intensity mechanism. By contrast, upon breaking centrosymmetry, Ru 5p–4d mixing allows for introduction of electric dipole allowed character resulting in a dramatic increase in the pre-edge intensity. The information content of this approach is explored as it relates to complexes of importance in olefin metathesis and its relevance as a tool for the study of reactive intermediates.

© 2007 Elsevier B.V. All rights reserved.

Keywords: Ruthenium complexes; X-ray absorption spectroscopy; Olefin metathesis; Assignment of pre-edge features; Electronic and geometric structure

1. Introduction

Analysis of the edge and pre-edge regions of first-row transition metal K-edges has become an effective method for the evaluation of the electronic structure of metal ions and the geometry of the surrounding ligands. The pioneering work of Edward I. Solomon and his coworkers has provided a systematic and effective methodology for the use of metal K-edge X-ray absorption spectroscopy (XAS) as a tool for the analysis of the electronic structure of first-row transition metal complexes. In general, it has been shown that low energy pre-edge features are well-resolved from the edge and result from transitions into empty or partially-empty valence 3d orbitals on the metal centre. For example, ligand field and electronic structure effects on the pre-edge features of a large number of Fe complexes have been systematically explored and assigned [1]. These

metal 3d \leftarrow 1s transitions are formally electric dipole forbidden for centrosymmetric molecules and are correspondingly very weak in octahedral compounds where electric quadrupole contributions dominate the intensity mechanism. However, distortions that break centrosymmetry can permit 4p mixing into the empty 3d orbitals, providing for electric dipole allowed character into the metal 3d \leftarrow 1s transitions, i.e., introduction of metal 4p \leftarrow 1s character. Electric quadrupole 3d \leftarrow 1s transitions are expected to contribute slightly to the pre-edge intensity regardless of symmetry [2], but these transitions are known to be approximately two orders of magnitude less intense than dipole mechanisms [3,4]. For this reason, even small contributions from 4p to 3d mixing can have a dramatic influence on the overall intensity of the pre-edge feature. The intensities of pre-edge features in first-row transition metals are therefore extremely sensitive to the specific nature of the electronic structure of the metal centre and its local symmetry.

For heavier metals, rigorous analysis of edge and pre-edge features is generally considered more difficult given

* Corresponding author. Tel./fax: +1 604 822 3817.

E-mail address: pierre@chem.ubc.ca (P. Kennepohl).

the inherently poorer resolution at the K-edge as well as an expected decrease in the energy separation between pre-edge features and the edge jump associated with ionization of the core electron. However, the prevalence of heavier transition metals in biological and homogeneous catalysis suggests that similar information would be of great utility beyond the first-row transition metals. It has generally been assumed that the pre-edge features for second-row transition metals are due to $4d \leftarrow 1s$ transitions by analogy to first-row metals; although, in many cases, the possibility of $5p \leftarrow 1s$ transitions has not been excluded [5–8]. More detailed studies of Mo [9] and Pd [10] K-edges have provided reasonable assignment of pre-edge features for these metals as due to metal $4d \leftarrow 1s$ transitions.

Ruthenium has found tremendous utility as a versatile late transition metal centre capable of mediating a number of important reactions. Most notably, the success of Ru carbene species as efficient catalysts in olefin metathesis has attracted significant attention over the last decade. Theoretical studies have investigated the nature of ruthenium catalysts [11–13], but somewhat surprisingly only sparing attention has been given to using spectroscopic approaches to provide detailed electronic structure insight into these key catalytic centres; a situation which has only recently been addressed [14–16]. In light of this, it is important to explore the information content that might be available through the investigation of Ru K-edge XAS. As a first step, we have endeavoured to provide data that would allow for the unambiguous assignment of Ru K-edge pre-edge features. Additionally, we are exploring the possibility of using these features as a tool for the elucidation of geometric and electronic structure information in a manner analogous to that which has been done for Fe K-edge XAS.

Our efforts have predominantly focused on the investigation of ruthenium organometallic complexes of relevance to olefin metathesis; therefore, this study includes a series of Grubbs-type complexes of both first (**a**: $L = \text{PCy}_3$) and second (**b**: $L = \text{H}_2\text{IMes}$) generations (Scheme 1). The square-pyramidal Grubbs complexes [17,18] (**1a,b**) as well as three related classes of compounds were examined (Table 1). Relative to the Grubbs complexes, the Piers phosphonium alkylidenes [19] (**2a,b**) have a phosphine transferred onto the alkylidene carbon while the Heppert carbides [20] (**3a,b**) contain a triple bonded carbide in place

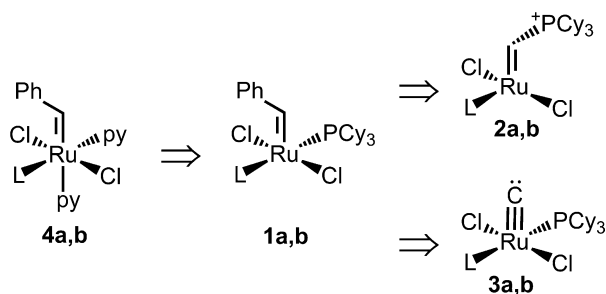
of the benzylidene. Two pyridine ligands replace one phosphine resulting in the octahedral Grubbs bispyridine complexes [21,22] (**4–7a,b**). The pyridines are mono-substituted as follows: py = pyridine (**4a,b**); 3-bromopyridine (**5a,b**); 3-nitropyridine (**6a,b**); or 4-methoxypyridine (**7a,b**). Our data indicate a clear relationship between the intensity of experimentally observed pre-edge features and the geometry at the metal centre, which allows for an unambiguous assignment of the pre-edge features and provides clues as to the type of information that may be available from the analysis of Ru K-edge XAS in the investigation of Ru carbenes in catalysis. In particular, Ru pre-edge features should be instructive regarding the geometry of reactive intermediates in the olefin metathesis cycle.

2. Results and discussion

Ru K-edge XAS data were obtained for 14 ruthenium compounds related to the Grubbs precatalysts. A pre-edge feature is observed in all complexes, although its intensity varies significantly over the range of complexes investigated. The normalised spectra clearly indicate that the pre-edge feature is extremely sensitive to geometry. Both the first generation (**a**: $L = \text{PCy}_3$, Fig. 1a) and second generation (**b**: $L = \text{H}_2\text{IMes}$, Fig. 1b) complexes follow the same trend of pre-edge feature intensity as follows: **4–7a,b** \ll **1a,b** $<$ **2a,b** \ll **3a,b** (Table 1).

It would seem reasonable, by analogy to previously investigated systems, that the pre-edge feature must result from bound-state (i.e. localized) transitions to low-lying valence states. Probable candidates include electric dipole forbidden Ru $4d \leftarrow 1s$ transitions and electric dipole allowed Ru $5p \leftarrow 1s$ transitions. The latter case might be considered most appropriate given that one would generally expect only small energy differences between the second-row transition metal $4d$ and $5p$ orbitals, suggesting that the weak electric dipole forbidden $4d \leftarrow 1s$ features might be overwhelmed by more intense $5p \leftarrow 1s$ features. It is key to note, however, that transitions to $4d$ and $5p$ final states are expected to behave very differently as a function of geometry and electronic structure. For example, and most importantly, the intensity of pre-edge features due to fully allowed metal $5p \leftarrow 1s$ transitions should be relatively independent of geometry whereas metal $4d \leftarrow 1s$ transitions are expected to be extremely sensitive to symmetry since small contributions from $5p$ mixing into the $4d$ orbitals would have a dramatic effect on the intensity of the feature.

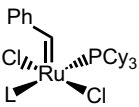
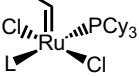
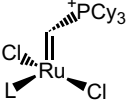
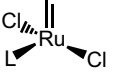
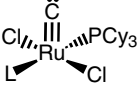
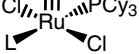
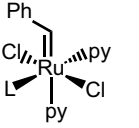
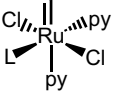
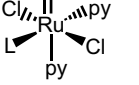
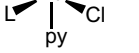
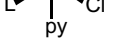

The six-coordinate pseudo-octahedral bispyridine complexes (**4–7a,b**) exhibit only very weak pre-edge features, in agreement with the expected behaviour of electric quadrupole allowed/electric dipole forbidden Ru $4d \leftarrow 1s$ transitions. In the octahedral limit, the symmetry of the empty $4d_{\sigma^*}$ orbitals prevents mixing with the $5p$ orbitals, enforcing the dipole forbidden nature of the transitions. Notably, these complexes exhibit a single pre-edge feature (no splitting of the empty $4d_{\sigma^*}$ orbitals) as would be



Scheme 1. Ruthenium complexes studied where (**a**) $L = \text{PCy}_3$ (tricyclohexylphosphine) or (**b**) H_2IMes (1,3-bis(2,4,6-trimethylphenyl)-4,5-dihydroimidazol-2-ylidene).

Table 1

Complexes with coordination number, approximate symmetry, and the area and energy of the pre-edge features. (a) L = PCy₃ and (b) L = H₂IMes

Complex L = PCy ₃ (a) or H ₂ IMes (b)	Coord. number	Approximate symmetry	Pre-edge area	Pre-edge energy (eV)
	5	C _{4v}	1.9	22116.4
	5	C _{4v}	1.8	22116.9
	4	C _s	1.7 ^a	22117.1
	4	C _s	2.3 ^a	22117.5
	5	C _{4v}	2.7	22118.4
	5	C _{4v}	3.0	22118.8
	6	O _h	1.0	22117.7
	6	O _h	1.0	22117.5
	6	O _h	1.0	22117.6
	6	O _h	1.3	22117.5
	6	O _h	1.1	22117.6
	6	O _h	1.1	22117.4
	6	O _h	1.0	22117.5
	6	O _h	1.1	22117.4

py = pyridine (**4a,b**);
 3-bromopyridine (**5a,b**);
 3-nitropyridine (**6a,b**);
 4-methoxypyridine (**7a,b**)

^a The edges in these cases were significantly broader than for other complexes; thus, constraints on the edge widths for **2a,b** were used. See [Supporting Information](#) for additional details.

expected for an octahedral low-spin d⁶ system with a single available ²E ligand field excited state [1].

Lower symmetry complexes exhibit very different pre-edge behaviour. For instance, the five-coordinate Grubbs complexes (**1a,b**) have significantly greater intensity in their pre-edge features, in accordance with the loss of centrosymmetry resulting from the absence of a ligand along the Ru=C axis (relative to the bipyridine species). Loss of an additional ligand, as exemplified by the Piers phosphonium alkylidenes (**2a,b**), generates a different type of distortion with similar intensity of the pre-edge feature. If, by contrast, the apical benzylidene ligand in **1a,b** is replaced with a terminal carbide, as in **3a,b**, the effect is a substantial increase in the pre-edge intensity. This effect corresponds with the much shorter M–C bond in the triply-bonded carbides (**3b**: 1.650 Å [20]) as compared to the benzylidenes (**1a**: 1.838 Å [21], **1b**: 1.835 Å [23], **4b**: 1.873 Å [21]) and phosphonium alkylidenes (**2b**: 1.817 Å [19]).

Density functional calculations indicate significant contributions from the metal 5p orbital into the 4d orbital for complexes **1a,b** and **2a,b**, which also supports the assignment of the pre-edge feature as the 4d ← 1s transition. The nature of the mixing, however, differs in each of these cases as a function of the type of structural distortion. In the five-coordinate complexes (**1a,b**), the major distortion occurs along the Ru=C bond, which generates a square

pyramidal-like structure. Mixing of the 5p orbitals consequently occurs primarily along this axis in the form of 4d_{z²}–5p_z mixing and the equatorial 5p_{x,y} orbitals do not contribute significantly. By contrast, the four-coordinate complexes (**2a,b**) show significant mixing along two directions – along the Ru=C bond as well as along the Ru–L bond, *i.e.*, along the axis of the second “missing” ligand. In this case, only one 5p orbital (formally pointing towards the *trans*-chloride ligands) is not involved in 5p–4d mixing. This result is consistent with previously observed behaviour in iron complexes where the nature of the 4p–3d mixing is anisotropic and correlates with specific structural distortions [1].

This study provides the foundation for the investigation of non-isolable reactive intermediates and their electronic and geometric characterisation based on their Ru K-edge XAS pre-edge features in concert with other spectroscopic techniques. Given the nature of the Ru K-edge pre-edge transitions as described herein, it should be possible to evaluate the coordination number and geometry of key intermediates in the organometallic chemistry of Ru species relevant to catalysis. We are currently exploring the electronic and geometric structure of olefin metathesis intermediates – including the putative four-coordinate active catalyst as well as the recently isolated ruthenacyclobutane intermediate [24], for which little geometric or electronic information is available. The addition of Ru K-edge XAS

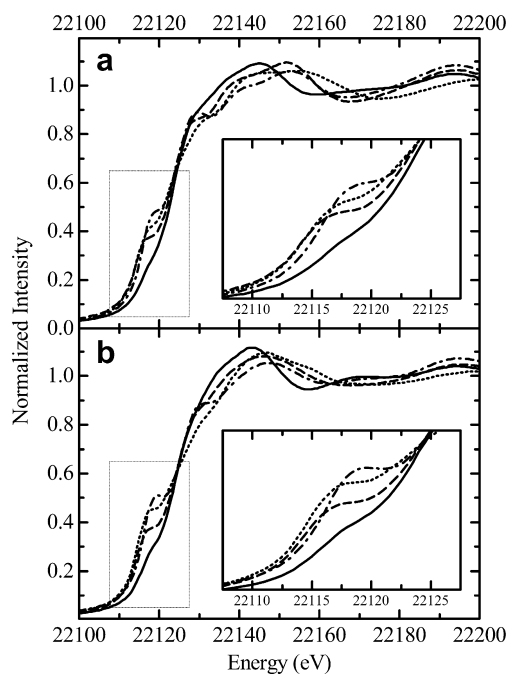


Fig. 1. Ru K-edge XAS spectra with insets showing expanded views of the pre-edge region for complexes (A) **1a** (—), **2a** (····), **3a** (---), and **4a** (-·-); and (B) **1b** (—), **2b** (····), **3b** (---), and **4b** (-·-).

pre-edge analysis as a tool in this effort should yield significant results.

3. Conclusions

Through examination of four classes of ruthenium compounds, we have established that the pre-edge feature in the Ru K-edge XAS spectra is due to formally electric dipole forbidden Ru 4d \leftarrow 1s transitions. Since this feature is extremely sensitive to geometry, it should be useful for determining unknown geometry for compounds such as the reactive intermediates in the olefin metathesis cycle.

4. Experimental details and methodology

4.1. General considerations

All storage and manipulations of compounds were carried out under an inert atmosphere of nitrogen using standard Schlenk line or glove box techniques. ^1H and ^{31}P NMR spectra were collected on a Bruker Avance 300 MHz spectrometer at ambient temperature. The following abbreviations are used below: s = singlet, d = doublet, t = triplet, m = multiplet, and br = broad signal. Elemental analyses were performed with a Carlo Erba EA 1108 elemental analyzer.

4.2. Materials

Toluene, ether and pentane were dried by passage through solvent purification columns. Complexes **1a** and **1b**, pyridine- d_5 , and anhydrous pyridine were purchased

from Sigma–Aldrich and used as received. Ampoules of methylene chloride- d_2 were purchased from Cambridge Isotope Laboratories and used as received. 3-Bromopyridine was purchased from AlfaAesar and 4-methoxypyridine was purchased from Sigma–Aldrich; both were dried over 4 Å molecular sieves. 4-Nitropyridine was purchased from AlfaAesar and dried under vacuum. Compounds **2a**, **2b**, **3a**, and **3b** were synthesized as described elsewhere [19,20] and obtained from Warren E. Piers.

4.3. Synthesis

The bispyridine complexes (**4–7a** and **4–7b**) were synthesised similarly to published procedures [21,22,25] for **4a**, **4b**, and **5b** by adding an excess of the appropriate pyridine to complexes **1a** or **1b**.

4.4. $[(\text{PCy}_3)(\text{py})_2(\text{Cl})_2\text{Ru}=\text{CHPh}]$ (**4a**)

Pyridine (2.0 mL, 25 mmol) was added to **1a** (0.2015 g, 0.2448 mmol) in a 20 mL vial (no other solvent used). The mixture was stirred at ambient temperature for 10 min and a colour change from purple to green was observed. Room temperature pentane (15 mL) was added and a precipitate began to form. The vial was capped and stored in a freezer (-25°C) overnight. The precipitate was vacuum-filtered, washed four times with 5 mL room temperature pentane, and dried under vacuum. The green solid **4a** was collected in 72% yield (0.1229 g, 0.1754 mmol). $^{31}\text{P}\{^1\text{H}\}$ NMR (CD_2Cl_2): δ 36.90 (s). ^1H NMR (CD_2Cl_2): δ 19.90 (d, 1H, CHPh , $J_{\text{HP}} = 11.7$ Hz), 8.74 (br, s, 2H, pyridine), 8.38 (br, s, 2H, pyridine), 7.93 (d, 2H, *ortho* CH, $J_{\text{HH}} = 7.3$ Hz), 7.64 (br, s, 2H, pyridine), 7.54 (t, 1H, *para* CH, $J_{\text{HH}} = 7.3$ Hz), 7.29 (br, s, 2H, pyridine), 7.18 (t, 2H, *meta* CH, $J_{\text{HH}} = 7.7$ Hz), 7.11 (br, s, 2H, pyridine), 2.42–1.01 (br, multiple peaks, 33H, $\text{P}(\text{C}_6\text{H}_{11})_3$). Anal. Calc. for $\text{C}_{35}\text{H}_{49}\text{Cl}_2\text{N}_2\text{PRu}$: C, 59.99; H, 7.05; N, 4.00. Found: C, 60.37; H, 7.12; N, 4.05%.

4.5. $[(\text{PCy}_3)(3\text{-Br-py})_2(\text{Cl})_2\text{Ru}=\text{CHPh}]$ (**5a**)

3-Bromopyridine (1.0 mL, 10 mmol) was added to **1a** (0.0978 g, 0.1188 mmol) in a 20 mL vial (no other solvent used). The mixture was stirred at ambient temperature for 10 min and a colour change from purple to green was observed. Room temperature pentane (15 mL) was added and a precipitate began to form. The vial was capped and stored in a freezer (-25°C) overnight. The precipitate was vacuum-filtered, washed four times with 5 mL room temperature pentane, and dried under vacuum. The green solid **5a** was collected in 71% yield (0.0723 g, 0.0842 mmol). $^{31}\text{P}\{^1\text{H}\}$ NMR (CD_2Cl_2): δ 38.78 (s). ^1H NMR (CD_2Cl_2): δ 19.70 (d, 1H, CHPh , $J_{\text{HP}} = 11.3$ Hz), 8.65 (br, s, 2H, pyridine), 8.48 (br, s, 2H, pyridine), 7.85 (d, 4H, *ortho* CH, $J_{\text{HH}} = 7.7$ Hz, pyridine), 7.54 (t, 1H, *para* CH, $J_{\text{HH}} = 7.1$ Hz), 7.20 (t, 4H, *meta* CH, $J_{\text{HH}} = 7.3$ Hz, pyridine), 2.44–1.07 (br, multiple peaks, 33H, $\text{P}(\text{C}_6\text{H}_{11})_3$). Anal.

Calc. for $C_{35}H_{47}Cl_2N_2Br_2PRu$: C, 48.97; H, 5.52; N, 3.26. Found: C, 49.32; H, 5.50; N, 3.26%.

4.6. $[(PCy_3)(3-NO_2-py)_2(Cl)_2Ru=CHPh]$ (**6a**)

3-Nitropyridine (0.7456 g, 6.008 mmol) was added to **1a** (0.1009 g, 0.1226 mmol) dissolved in 2 mL toluene in a 20 mL vial. The mixture was stirred at ambient temperature for 10 min and a colour change from purple to brown was observed. Room temperature pentane (15 mL) was added and a precipitate began to form. The vial was capped and stored in a freezer (-25°C) overnight. The precipitate was vacuum-filtered, washed four times with 5 mL room temperature pentane, washed two times with 5 mL room temperature ether to remove excess solid 3-nitropyridine, and dried under vacuum. The brown solid **6a** was collected in 35% yield (0.0341 g, 0.0431 mmol). $^{31}\text{P}\{^1\text{H}\}$ NMR (CD_2Cl_2): δ 39.55 (s). ^1H NMR (CD_2Cl_2): δ 19.67 (d, 1H, $CHPh$, $J_{HP} = 11.3$ Hz), 9.42 (br, s, 2H, pyridine), 8.91 (br, s, 2H, pyridine), 8.45 (d, 2H, *ortho* CH, $J_{HH} = 6.7$ Hz), 7.79 (d, 2H, *para* CH, $J_{HH} = 6.9$ Hz, pyridine), 7.48 (br, s, 3H, pyridine), 7.15 (t, 2H, *meta* CH, $J_{HH} = 7.1$ Hz), 2.44–1.10 (br, multiple peaks, 33H, $\text{P}(\text{C}_6\text{H}_{11})_3$). Anal. Calc. for $C_{35}H_{47}Cl_2N_4O_4PRu$: C, 53.16; H, 5.99; N, 7.09. Found: C, 53.15; H, 5.99; N, 7.12%.

4.7. $[(PCy_3)(4-OMe-py)_2(Cl)_2Ru=CHPh]$ (**7a**)

3-Methoxypyridine (0.5 mL, 4.9 mmol) was added to **1a** (0.1027 g, 0.1248 mmol) dissolved in 1 mL toluene in a 20 mL vial. The mixture was stirred at ambient temperature for 10 min and a colour change from purple to green was observed. Room temperature pentane (15 mL) was added and a precipitate began to form. The vial was capped and stored in a freezer (-25°C) overnight. The precipitate was vacuum-filtered, washed four times with 5 mL room temperature pentane, and dried under vacuum. The green solid **7a** was collected in 47% yield (0.0450 g, 0.0591 mmol). $^{31}\text{P}\{^1\text{H}\}$ NMR (CD_2Cl_2): δ 35.96 (s). ^1H NMR (CD_2Cl_2): δ 19.97 (d, 1H, $CHPh$, $J_{HP} = 11.7$ Hz), 8.63 (br, s, 2H, pyridine), 8.17 (br, s, 2H, pyridine), 7.99 (d, 2H, *ortho* CH, $J_{HH} = 7.7$ Hz), 7.56 (t, 1H, *para* CH, $J_{HH} = 7.1$ Hz), 7.20 (t, 2H, *meta* CH, $J_{HH} = 7.7$ Hz), 6.83 (br, s, 2H, pyridine), 6.58 (br, s, 2H, pyridine), 3.85 (s, 3H, OCH_3), 3.78 (s, 3H, OCH_3), 2.39–1.00 (br, multiple peaks, 33H, $\text{P}(\text{C}_6\text{H}_{11})_3$). Anal. Calc. for $C_{37}H_{53}Cl_2N_2O_2PRu$: C, 58.41; H, 7.02; N, 3.68. Found: C, 58.76; H, 7.04; N, 3.75%.

4.8. $[(H_2IMes)(py)_2(Cl)_2Ru=CHPh]$ (**4b**)

Pyridine (1.0 mL, 12 mmol) was added to **1b** (0.0998 g, 0.1176 mmol) dissolved in 1 mL toluene in a 20 mL vial. The mixture was stirred at ambient temperature for 10 min and a colour change from red to green was observed. Room temperature pentane (15 mL) was added and a precipitate began to form. The vial was capped and stored in a freezer (-25°C) overnight. The precipitate

was vacuum-filtered, washed four times with 5 mL room temperature pentane, and dried under vacuum. The green solid **4b** was collected in 53% yield (0.0455 g, 0.0626 mmol). ^1H NMR (CD_2Cl_2): δ 19.14 (s, 1H, $CHPh$),¹ 8.61 (br, s, 2H, pyridine), 7.79 (d, 2H, pyridine), 7.67 (br, s, 1H, pyridine), 7.59 (d, 2H, *ortho* CH, $J_{HH} = 7.7$ Hz), 7.49 (t, 2H, *para* CH, $J_{HH} = 7.3$ Hz, pyridine), 7.26 (br, s, 2H, pyridine), 7.08 (t, 2H, *meta* CH, $J_{HH} = 7.7$ Hz), 7.03–6.70 (br, multiple peaks, 6H, Mes CH, pyridine), 4.09 (br, d, 4H, $\text{NCH}_2\text{CH}_2\text{N}$), 2.69–2.14 (br, multiple peaks, 18H, Mes CH_3). Anal. Calc. for $C_{38}H_{42}Cl_2N_4Ru$: C, 62.80; H, 5.83; N, 7.71. Found: C, 62.77; H, 6.10; N, 7.88%.

4.9. $[(H_2IMes)(3-Br-py)_2(Cl)_2Ru=CHPh]$ (**5b**)

3-Bromopyridine (1.0 mL, 10 mmol) was added to **1b** (0.0993 g, 0.1170 mmol) dissolved in 1 mL toluene in a 20 mL vial. The mixture was stirred at ambient temperature for 10 min and a colour change from red to green was observed. Room temperature pentane (15 mL) was added and a precipitate began to form. The vial was capped and stored in a freezer (-25°C) overnight. The precipitate was vacuum-filtered, washed four times with 5 mL room temperature pentane, and dried under vacuum. The green solid **5b** was collected in 55% yield (0.0564 g, 0.0638 mmol). ^1H NMR (CD_2Cl_2): δ 19.07 (s, 1H, $CHPh$),¹ 8.65 (br, d, 2H, pyridine), 8.00 (br, s, 1H, pyridine), 7.74 (br, s, 2H, pyridine), 7.60 (d, 2H, *ortho* CH, $J_{HH} = 7.3$ Hz), 7.49 (t, 1H, *para* CH, $J_{HH} = 7.1$ Hz), 7.09 (t, 3H, *meta* CH, $J_{HH} = 7.5$ Hz, pyridine), 7.00–6.76 (br, multiple peaks, 6H, Mes CH, pyridine), 4.07 (br, d, 4H, $\text{NCH}_2\text{CH}_2\text{N}$), 2.69–2.14 (br, multiple peaks, 18H, Mes CH_3). Anal. Calc. for $C_{38}H_{42}Cl_2N_4Ru$: C, 62.80; H, 5.83; N, 7.71. Found: C, 62.77; H, 6.10; N, 7.88%.

4.10. $[(H_2IMes)(3-NO_2-py)_2(Cl)_2Ru=CHPh]$ (**6b**)

3-Nitropyridine (0.7223 g, 5.820 mmol) was added to **1b** (0.1056 g, 0.1244 mmol) dissolved in 2 mL toluene in a 20 mL vial. The mixture was stirred at ambient temperature for 10 min and a colour change from red to brown was observed. Room temperature pentane (15 mL) was added and a precipitate began to form. The vial was capped and stored in a freezer (-25°C) overnight. The precipitate was vacuum-filtered, washed four times with 5 mL room temperature ether to remove excess solid 3-nitropyridine, washed once with 5 mL room temperature pentane, and dried under vacuum. The brown solid **6b** was collected in 50% yield (0.0513 g, 0.0628 mmol). ^1H NMR (CD_2Cl_2):

¹ The ^1H NMR spectra of complexes **4b**, **5b** and **6b** contain a second small singlet (<5%) in the alkylidene region (18.53 ppm), which is likely due to the monopyridine adduct $[(H_2IMes)(py)(Cl)_2Ru=CHPh]$. The solid samples analyze as the bipyridine complexes and the signal is not present when pyridine- d_5 is used as the NMR solvent, suggesting that one pyridine ligand is somewhat more labile than the other; a finding that is consistent with previous reports [21,23].

δ 19.05 (s, 1H, *CHPh*), 1 9.21 (br, d, 3H, pyridine), 8.34 (br, t, 3H, pyridine), 7.59 (d, 2H, *ortho CH*, $J_{\text{HH}} = 8.1$ Hz), 7.46 (t, 2H, *para CH*, $J_{\text{HH}} = 7.1$ Hz, pyridine), 7.06 (t, 3H, *meta CH*, $J_{\text{HH}} = 7.7$ Hz, pyridine), 6.81 (d, 4H, Mes *CH*), 4.07 (br, s, 4H, $\text{NCH}_2\text{CH}_2\text{N}$), 2.66–2.18 (br, multiple peaks, 18H, Mes CH_3). *Anal.* Calc. for $\text{C}_{38}\text{H}_{40}\text{Cl}_2\text{N}_6\text{O}_4\text{Ru}$: C, 55.88; H, 4.94; N, 10.29. Found: C, 55.70; H, 5.15; N, 10.17%.

4.11. $[(\text{H}_2\text{IMes})(4\text{-OMe-py})_2(\text{Cl})_2\text{Ru}=\text{CHPh}]$ (**7b**)

3-Methoxypyridine (0.5 mL, 4.9 mmol) was added to **1b** (0.0990 g, 0.1166 mmol) dissolved in 1 mL toluene in a 20 mL vial. The mixture was stirred at ambient temperature for 10 min and a colour change from red to green was observed. Room temperature pentane (15 mL) was added and a precipitate began to form. The vial was capped and stored in a freezer (-25°C) overnight. The precipitate was vacuum-filtered, washed four times with 5 mL room temperature pentane, and dried under vacuum. The green solid **7b** was collected in 69% yield (0.0633 g, 0.0805 mmol). ^1H NMR (CD_2Cl_2): δ 19.11 (d, 1H, *CHPh*, $J_{\text{HH}} = 7.7$ Hz), 8.43 (br, s, 2H, pyridine), 7.73–6.48 (br, multiple peaks, 15H, *ortho*, *meta*, *para CH*, Mes *CH*, pyridine), 4.09 (br, d, 4H, $\text{NCH}_2\text{CH}_2\text{N}$), 3.85 (d, 3H, OCH_3 , $J_{\text{HH}} = 8.1$ Hz), 3.74 (d, 3H, OCH_3 , $J_{\text{HH}} = 7.7$ Hz), 2.75–2.13 (br, multiple peaks, 18H, Mes CH_3). *Anal.* Calc. for $\text{C}_{40}\text{H}_{46}\text{Cl}_2\text{N}_4\text{O}_2\text{Ru}$: C, 61.06; H, 5.89; N, 7.12. Found: C, 61.35; H, 6.16; N, 6.99%.

4.12. XAS sample preparation

All sample preparation was performed in a nitrogen-filled glove box and samples were kept in an inert atmosphere or frozen in liquid nitrogen prior to and during data acquisition. Each solid was diluted approximately sevenfold with boron nitride and the mixture was gently ground for >5 min using a mortar and pestle to generate homogeneous, finely dispersed powders. Each mixture was then pressed into a 0.5 mm thick aluminium spacer that was sealed on both sides with Kapton tape.

4.13. XAS data acquisition

Ru K-edge X-ray absorption spectroscopic data were collected at the Stanford Synchrotron Radiation Laboratory (SSRL) on beamline 7–3 under ring conditions 80–100 mA at 3.0 GeV. This beamline has a 20-pole, 2 T wiggler, 0.8 mrad beam and a Si (220) double-crystal monochromator that was detuned by 50% intensity to minimise higher harmonic contamination. The incident X-ray intensity (I_0), sample absorption (I_1), and Ru reference absorption (I_2) were measured as transmittance in three consecutive argon-filled ionization chambers and fluorescence data were collected using a 30-element Ge detector array. Two to four sweeps were taken for each sample and all data were measured to $k = 18 \text{ \AA}^{-1}$ at $13 \pm 3 \text{ K}$

within an Oxford Instruments CF1208 continuous-flow liquid helium cryostat.

4.14. XAS data processing

X-ray absorption data were processed using the SIXPACK software package developed by Sam Webb at SSRL [26]. Transmission and fluorescence data consistently yielded similar edge and pre-edge features; transmission data are reported throughout. All identical transmission sweeps for a complex were averaged and energy calibrated using the internal reference spectra of Ru foil, with the lowest energy inflection point assigned as 22117 eV. Background subtraction and normalization were performed simultaneously using a linear pre-edge function and a quadratic post-edge function.

The commercially available PEAKFIT® software package [27] was used to model the pre-edge region with a single Voigt amplitude function and the ionization edge feature with a cumulative Gaussian/Lorentzian function. The spectra were fit over the energy region from 22090 eV to 22128 eV. The pre-edge features were generally well modelled with a fixed 1:1 ratio of Gaussian:Lorentzian shapes. Edge features were well modelled with a fixed 1:1 ratio of cumulative Gaussian:Lorentzian shapes while varying the amplitude, peak position and width of Gaussian and Lorentzian shapes.

4.15. Computational details

Geometry optimizations followed by ground state DFT calculations for compounds **1a,b** and **2a,b** were performed using the Vosko-Wilk-Nusair local density approximation with exchange and correlation corrections from Becke [28] and Perdew [29,30], respectively (BP86). Slater-type orbitals [31] (STOs) were used for the triple zeta basis set with an additional set of polarization functions (TZP). The $[\text{Ar}]^{18}\text{d}^{10}$ core electrons of ruthenium were treated by the frozen core approximation [32]. The calculations were carried out with the program package ADF.2005 [33–35]. The run files corresponding to the ground state calculation of complexes **1a,b** and **2a,b** are provided as [Supplementary information](#).

Acknowledgements

This research is funded by NSERC (Canada). Start-up funds and infrastructure support provided by UBC. Calculations were performed on computational infrastructure funded by the Canada Foundation for Innovation (CFI) and the British Columbia Knowledge Development Fund (BCKDF) through the Centre for Higher Order Structure Elucidation (CHORSE). Special thanks to Dr. Warren Piers at the University of Calgary for providing compounds **2a, b** and **3a, b**. We appreciate the technical and scientific support provided by Dr. Serena DeBeer George during data collection at the Stanford Synchrotron Radia-

tion Laboratory (SSRL). We recognise Dr. Sam Webb (SSRL) for his assistance with the sixpack software. Portions of this research were carried out at SSRL, a national user facility operated by Stanford University on behalf of the U.S. DOE-BES. The SSRL Structural Molecular Biology Program is supported by DOE, Office of Biological and Environmental Research, and by the NIH, National Center for Research Resources, Biomedical Technology Program.

Appendix A. Supplementary material

Supplementary data associated with this article can be found, in the online version, at [doi:10.1016/j.ica.2007.07.029](https://doi.org/10.1016/j.ica.2007.07.029).

References

- [1] T.E. Westre, P. Kennepohl, J.G. DeWitt, B. Hedman, K.O. Hodgson, E.I. Solomon, *J. Am. Chem. Soc.* 119 (1997) 6297–6314.
- [2] J.E. Hahn, R.A. Scott, K.O. Hodgson, S. Doniach, S.R. Desjardins, E.I. Solomon, *Chem. Phys. Lett.* 88 (1982) 595–598.
- [3] R.A. Bair, W.A. Goddard, *Phys. Rev. B* 22 (1980) 2767.
- [4] C. Brouder, *J. Phys.: Condens. Matter* 2 (1990) 701.
- [5] V.O. Kostroun, R.W. Fairchild, C.A. Kukkonen, J.W. Wilkins, *Phys. Rev. B* 13 (1976) 3268.
- [6] C.M. Wang, G.S. Cargill III, H.M. Chan, M.P. Harmer, *J. Am. Ceram. Soc.* 85 (2002) 2492–2498.
- [7] T. Ressler, O. Timpe, T. Neisius, J. Find, G. Mestl, M. Dieterle, R. Schlogl, *J. Catal.* 191 (2000) 75–85.
- [8] K. Okamoto, J. Miyawaki, K. Nagai, D. Matsumura, A. Nojima, T. Yokoyama, H. Kondoh, T. Ohta, *Inorg. Chem.* 42 (2003) 8682–8689.
- [9] C.E. Laplaza, M.J.A. Johnson, J.C. Peters, A.L. Odom, E. Kim, C.C. Cummins, G.N. George, I.J. Pickering, *J. Am. Chem. Soc.* 118 (1996) 8623–8638.
- [10] M. Tromp, J.A. vanBokhoven, G.P.F. vanStrijdonck, P.W.N.M. vanLeeuwen, D.C. Koningsberger, D.E. Ramaker, *J. Am. Chem. Soc.* 127 (2005) 777–789.
- [11] C. Adlhart, P. Chen, *Angew. Chem., Int. Ed.* 41 (2002) 4484–4487.
- [12] C. Adlhart, P. Chen, *Helv. Chim. Acta* 86 (2003) 941–949.
- [13] A. Krapp, K.K. Pandey, G. Frenking, *J. Am. Chem. Soc.* 129 (2007) 7596–7610.
- [14] C.Y. Wong, M.C.W. Chan, N. Zhu, C.M. Che, *Organometallics* 23 (2004) 2263–2272.
- [15] M.U. Delgado-Jaime, J.C. Conrad, D.E. Fogg, P. Kennepohl, *Inorg. Chim. Acta* 359 (2006) 3042–3047.
- [16] K. Getty, M.U. Delgado-Jaime, P. Kennepohl, unpublished results.
- [17] P. Schwab, R.H. Grubbs, J.W. Ziller, *J. Am. Chem. Soc.* 118 (1996) 100–110.
- [18] M. Scholl, S. Ding, C.W. Lee, R.H. Grubbs, *Org. Lett.* 1 (1999) 953–956.
- [19] P.E. Romero, W.E. Piers, R. McDonald, *Angew. Chem., Int. Ed.* 43 (2004) 6161–6165.
- [20] R.G. Carlson, M.A. Gile, J.A. Heppert, M.H. Mason, D.R. Powell, D.V. Velde, J.M. Vilain, *J. Am. Chem. Soc.* 124 (2002) 1580–1581.
- [21] M.S. Sanford, J.A. Love, R.H. Grubbs, *Organometallics* 20 (2001) 5314–5318.
- [22] T.M. Trnka, E.L. Dias, M.W. Day, R.H. Grubbs, *Arkivoc* 13 (2002) 28–41.
- [23] J.A. Love, M.S. Sanford, M.W. Day, R.H. Grubbs, *J. Am. Chem. Soc.* 125 (2003) 10103–10109.
- [24] P.E. Romero, W.E. Piers, *J. Am. Chem. Soc.* 127 (2005) 5032–5033.
- [25] J.A. Love, J.P. Morgan, T.M. Trnka, R.H. Grubbs, *Angew. Chem., Int. Ed.* 41 (2002) 4035–4037.
- [26] S.M. Webb, *Phys. Scripta* T115 (2005) 1011–1014.
- [27] PEAKFIT 4.12; SeaSolve Software Inc. 2003.
- [28] A.D. Becke, *Phys. Rev. A* 38 (1988) 3098.
- [29] J.P. Perdew, *Phys. Rev. B* 34 (1986) 7406.
- [30] J.P. Perdew, *Phys. Rev. B* 33 (1986) 8822.
- [31] J.G. Snijders, E.J.A. Baerdens, *Data Nucl. Data Tables* 26 (1982) 483–509.
- [32] E.J. Baerdens, D.E. Ellis, P. Ros, *Chem. Phys.* 2 (1973) 41–51.
- [33] ADF2005.01 Theoretical Chemistry, Vrije Universiteit: Amsterdam, The Netherlands.
- [34] C.F. Guerra, J.G. Snijders, G. te Velde, E.J. Baerdens, *Theor. Chem. Acc.* 99 (1998) 391–403.
- [35] G. te Velde, F.M. Bickelhaupt, E.J. Baerends, C. Fonseca Guerra, S.J.A. van Gisbergen, J.G. Snijders, T.J. Ziegler, *Comp. Chem.* 22 (2001) 931–967.